How the materials knowledge of Roman mortars could be helpful for the production of future materials: The case of the *Aqua Traiana* aqueduct (Rome, Italy)

Laura Medeghini [a],*, Laura Calzolari [a], Sara Capriotti [a], Martina Bernabale [a], Caterina De Vito [a], Mauro Giustini [b], Ida Pettiti [b], Gianfranco Dell'Agli [c], Luca Spiridigliozzi [c], Amina Antonacci [d], Giulia Gasperuzzo [d], Viviana Scognamiglio [d], Valeria Di Tullio [e], Margherita Zappelli [e], Lucia Conti [f], Eleonora Gioventù [f], Marina Marcelli [g], Alfredo Bonaccini [h], Silvano Mignardi [a]

[a] *Department of Earth Sciences, Sapienza University of Rome, Piazzale Aldo Moro, 5, 00185 Rome, Italy*
[b] *Department of Chemistry, Sapienza University of Rome, Piazzale Aldo Moro, 5, 00185 Rome, Italy*
[c] *Department of Civil and Mechanical Engineering, University of Cassino and Southern Lazio, Via Di Biasio 43, 03043 Cassino, Frosinone, Italy*
[d] *Institute of Crystallography, National Research Council of Italy, Department of Chemical Sciences and Materials Technologies, Strada Provinciale 35d, 9, 00010 Montelibretti, Rome, Italy*
[e] *Institute of Heritage Science (ISPC), CNR, Via Salaria km 29, 300, Montelibretti, Rome, Italy*
[f] *Central Institute for Restoration (ICR), Via di San Michele 25, 00153 Rome, Italy*
[g] *Sovrintendenza Capitolina ai Beni Culturali, piazza Lovatelli, 35, 00186 Rome, Italy*
[h] *Tecno Edile Toscana Srl, Via Monti Lepini 14, 04100 Latina (LT), Italy*

ARTICLE INFO

ABSTRACT

Starting from the knowledge of ancient materials, the present work aims at developing green eco-friendly restoration mortars.

A multi-step approach is proposed for this purpose including a characterization of ancient mortars, followed by that of the raw materials, ending with an in-depth one of the new products.

Therefore, new mortars have been produced following the ancient recipe used in the construction of the *Aqua Traiana* aqueduct (Rome, 2nd century CE).

Minero-petrographic and mechanical features, along with the assessment of porosity, water absorption, hydraulic index, and the evaluation of phytotoxicity toward microalgae cells, have been considered to evaluate the new products.

The results proved that the nature of the aggregate and of the binder influence the porosity and the formation of newly reaction phases. The growth of these minerals creates a porous network inside the binder paste which shows an efficient reactivity in the formation of C-S-H compounds.

1. Introduction

Nowadays cement-based materials constitute the pillars of our new constructions, establishing themselves as the largest manufactured products worldwide. The demand for cement-based materials continues to rise, driven by the imperative for infrastructure repairs and the ongoing development of cities and new countries. However, this increased demand led to a concerning rise in cement production. Current estimates indicate that cement production contributes to approximately 7 % to 9 % of the planet-wide total CO_2 emissions, and if left unchecked, these emissions are expected to undergo an unacceptable increase [1,2], significantly affecting the environment. A potential approach to consider in mitigating the situation is drawing insights from the past. Indeed, analysing past impacts and responses in specific historical contexts can illuminate possibilities for effecting changes in the present. In the last decade, this approach was applied to various fields and proved to be an effective way to discover new solutions rooted in ancient knowledge. Therefore, the scientific community has redirected

its attention toward studying ancient materials and production methods to propose future perspectives for creating new, sustainable applications based on the science and usage recovered from the past. Ancient pigments with interesting photophysical properties have been studied for the production of optical sensing materials [3], ancient colourants for novel sustainable applications [4], the utilization of kaolin in porcelain for nanomaterials [5], modern applications of basalt fibres [6], ancient laminated composites [7] and ancient iron-based materials [8] to improve the features of modern materials.

As far as building materials is concerned, ancient Mexican stuccoes analysed in depth for restoration [9], bricks, stones and plaster as part of an eco-renovation of historic centres in France [10], and ceramic additives in mortars for producing more strength modern concrete materials [11] are just a few examples. The understanding of these materials and their ancient production techniques serves as a fundamental step toward the development of more sustainable practices for creating durable and resilient new materials [12].

Chemical and mineralogical characterization of ancient mortars have shown that ancient Roman buildings and infrastructures were skillfully crafted using hydraulic lime, volcanic products, and a variety of aggregates, contributing to their remarkable endurance over time [12–15]. Among the many Roman architectural wonders, their marine structures have garnered significant attention through extensive investigation [16–18]. These structures have demonstrated a lifespan of approximately two orders of magnitude longer than marine constructions relying on Portland cement [19].

However, it is crucial to emphasize that the presence of steel reinforcement in modern constructions stands as a primary cause of deterioration due to corrosion. Unlike the construction methods of ancient Romans, who did not employ steel reinforcement, the use of this material in contemporary structures can lead to premature degradation caused by natural corrosion processes [20,21]. Despite this significant difference in construction practices between ancient and modern times, it is important to consider that learning from the past could be valuable in planning alternative, sustainable, and enduring building techniques for the future. In this perspective, the realm of building restoration offers a promising avenue for the application and refinement of niche solutions, which can then be re-considered for wider modern applications. By focusing on restoration efforts, we can lay the groundwork for evaluating the modern applicability of these techniques and materials, paving the way for broader application in contemporary construction practices. In the production of new green building materials (i.e. eco-friendly and manufactured with energy reducing processes, designed to minimize its environmental impact respect to cement-based materials), the evaluation of the potential danger posed by construction materials on the environment represents a topic of recent interest [22–24]. The need to delve deeper into this issue arises from the influence of building materials on local environments by releasing hazardous substances [25] and heavy metals [26–28] which can be transported, accumulated, degraded, and even absorbed, by living organisms [29]. Furthermore, it is noteworthy that recent research promotes the creation of new mortars with the addition of specific additives (e.g. nanomaterials) or with the use of waste materials, to achieve goals related to greater durability and sustainability. In all these contexts, a phytotoxicity analysis on building materials is proving to be very interesting since it can make an important contribution as a valuable tool to evaluate if an environmental impact has to be expected [30,31]. Even if a technical report on the use of ecotoxicity testing on construction products was published for the first time in 2017 (CEN/TR 17105:2017 [32]), today the process for evaluating the potential toxicity of construction materials is complex and not so diffuse, nonetheless, it is increasingly considered of fundamental importance. In this view, the production of green mortars for the restoration niche represents a crucial first endeavour toward achieving a sustainable future in the field of building constructions.

Following the information gathered from the past, the present work aims at developing high performance, green and eco-friendly restoration mortars that are not harmful to humans and have less impact on the environment, preserving cultural heritage and the environment for future generations.

The starting point of this work was a chemical and mineralogical characterization of ancient hydraulic mortars from the inner duct of the *Aqua Traiana* aqueduct (Rome, 2nd century CE) which have allowed the monument to survive to the present day [33,34]. The monument, still used today, shows hard hydraulic mortars with an extraordinary resistance to decay processes.

The investigations highlighted that two types of mortars are present in the monument: one original dated back to the Trajan Age and the other connected to a restoration intervention by pope Paulus V (1609–1612) [33,34]. Both types of mortar are hard and compact, resistant and not friable, characterized by fine volcanic aggregate, mainly represented by pozzolan, tuff and lava fragments, ranging from fine sand to gravel-sized and corresponding to the Vitruvius *harena fossicia* [35]. The local supply from the Bracciano Lake (Rome, Italy) of the pozzolanic aggregate was inferred for both types of mortar [33]. The main difference between the two types is related to the binder fraction: Trajan samples show a calcite-free amorphous binder whereas papal samples show the expected typical calcitic lime binder [34]. Due to the high hydraulicity of both the Trajan and papal samples, it was possible to hypothesize that the starting raw material was a natural hydraulic one, e.g., from a limestone containing parts of clays [33,34].

Therefore, starting from a specific case study which shows high performance in terms of resistance and durability, new mortars have been produced following the multi-step approach here proposed for this purpose. A preliminary characterization of pozzolanic materials from the surrounding of Bracciano Lake (Rome, Italy) has been carried out. Subsequently, the pozzolanic materials with a similar composition observed in the ancient samples have been chosen for the new mortar recipes, which have been then analysed from a petrographic and mineralogical perspective. Additionally, porosity, compressive and flexural strength have also been considered to assess the physical and mechanical characteristics of the new products. Moreover, to fully support the idea of producing new mortars with minimal impact on the environment, the innovative evaluation of the phytotoxicity of new mortar specimens on microalgae cells has been included according to OECD (Organization for Economic Cooperation and Development) guidelines, that are currently used by government, industry, and independent laboratories for the identification of chemicals during the development of new products [36] (Fig. 1).

The focus of this study is to demonstrate how the knowledge of ancient materials and production technologies can be positively fused to generate new green mortars, which could be useful in modern applications.

2. Materials and methods

The methodological approach includes various steps (Fig. 1): 1) the chemical and mineralogical characterization of ancient mortars from the *Aqua Traiana* aqueduct; 2) the analysis of possible raw materials used in antiquity; 3) the production of experimental mortars starting from the ancient recipes and finally 4) a detailed characterization of the new materials to evaluate their possible use in the restoration field.

2.1. Analysis of the raw materials

After a survey of the pozzolan quarries in the surrounding of the Bracciano Lake, from where the provenance of the raw materials was hypothesised, three typologies of pozzolan were chosen. In detail, two pozzolan quarries (A and C) are in the northeastern part of the Lake (close to Vicarello) and one (B) in the southwest (close to Castel Giuliano) (Table 1).

Pozzolanic materials were analysed by a multi-analytical approach including thin section Optical Microscopy (OM), X-ray Powder
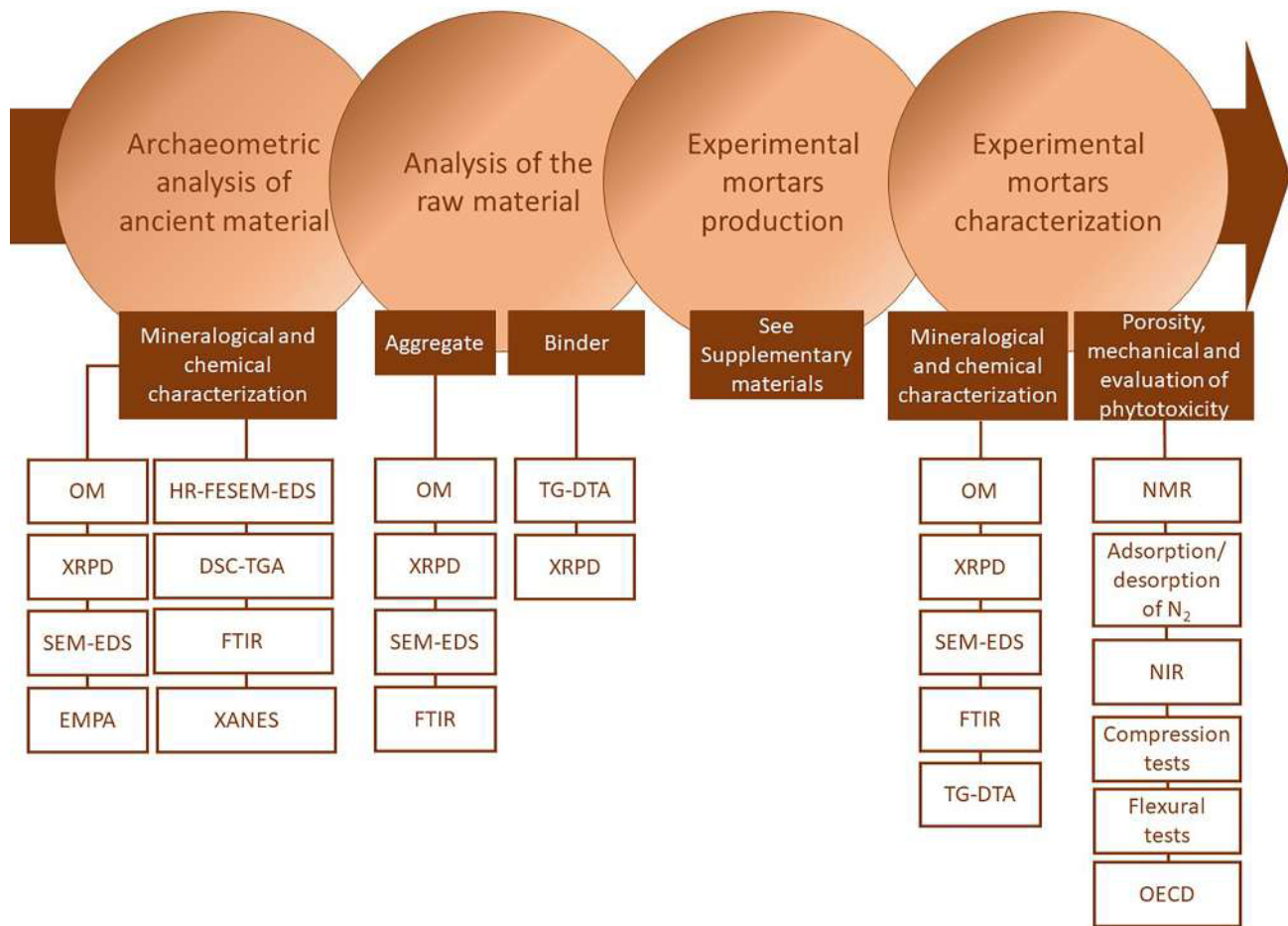
Fig. 1. The methodological approach proposed in the study (OM: thin section Optical Microscopy; XRPD: X-ray Powder Diffraction; SEM-EDS: Scanning Electron Microscopy coupled with Energy Dispersive X-ray Spectroscopy; EMPA: Electron Microprobe Analysis; HR-FESEM-EDS: High Resolution Field Emission Scanning Electron Microscopy; DSC-TGA: Differential Scanning Calorimetry coupled with Thermogravimetric Analysis; FTIR: Fourier-Transform Infrared Spectroscopy; XANES: X-ray Absorption Near Edge Structure Spectroscopy; TG-DTA: Thermogravimetry and Differential Thermal Analysis; NMR: Nuclear Magnetic Resonance Spectroscopy; NIR: Near Infrared Spectroscopy; OECD: the phytotoxicity test).

Table 1
Raw material properties.

Sample	Nature	Provenance	Colour	Grain size (mm)
A	Pozzolan	Northeastern part of the Bracciano Lake	Brown	<0.15–1.25
B	Pozzolan	Southwest part of the Bracciano Lake	Brown-gray	<0.15–2.36
C	Pozzolan	Northeastern part of the Bracciano Lake	Brown-red	<0.15–5

Sample	Nature	Brand	Colour	Compressive resistance after 28 days hardening (MPa)
NHL B	Natural hydraulic lime	Tecno Edile Toscana	White	>5
NHL D	Natural hydraulic lime	Tecno Edile Toscana	White	>3.5

Diffraction (XRPD), Scanning Electron Microscopy coupled with Energy Dispersive X-ray Spectroscopy (SEM-EDS) and Fourier-Transform Infrared Spectroscopy (FTIR).

In detail, thin section OM was used to investigate the mineralogical and textural composition of the samples. This analysis permits the assessment of the mineralogical nature, size of crystals, habit, abundance, alterations of the pozzolan materials, etc.

XRPD and FTIR were applied to define the minerals composing the samples.

SEM-EDS analyses were useful to study in detail the chemical composition of specific mineralogical phases. Elemental analysis was also used to analyse the distribution and abundance of selected elements and to characterize altered inclusions.

Based on the results of the chemical and mineralogical investigation of ancient mortars which suggested the use of a natural hydraulic binder [33,34], two different natural hydraulic lime, NHL B and NHL D, were chosen due to the declared mechanical properties (Table 1). Both NHLs were characterized by Thermogravimetry and Differential Thermal Analysis (TG-DTA) and XRPD to estimate the composition.

2.2. Production of the specimens

Based on the preliminary analytical results (see Section 3.1), pozzolans A and C were chosen as the aggregate of the specimens due to their composition close to those observed in the ancient mortars. The aggregate grain size was normalized by grinding and sieving between 150 μm and 5 mm, the different fractions were weighted (Fig. 2), and the grain size distribution was modified by adding the smaller fraction which was predominant in the archaeological samples [33].

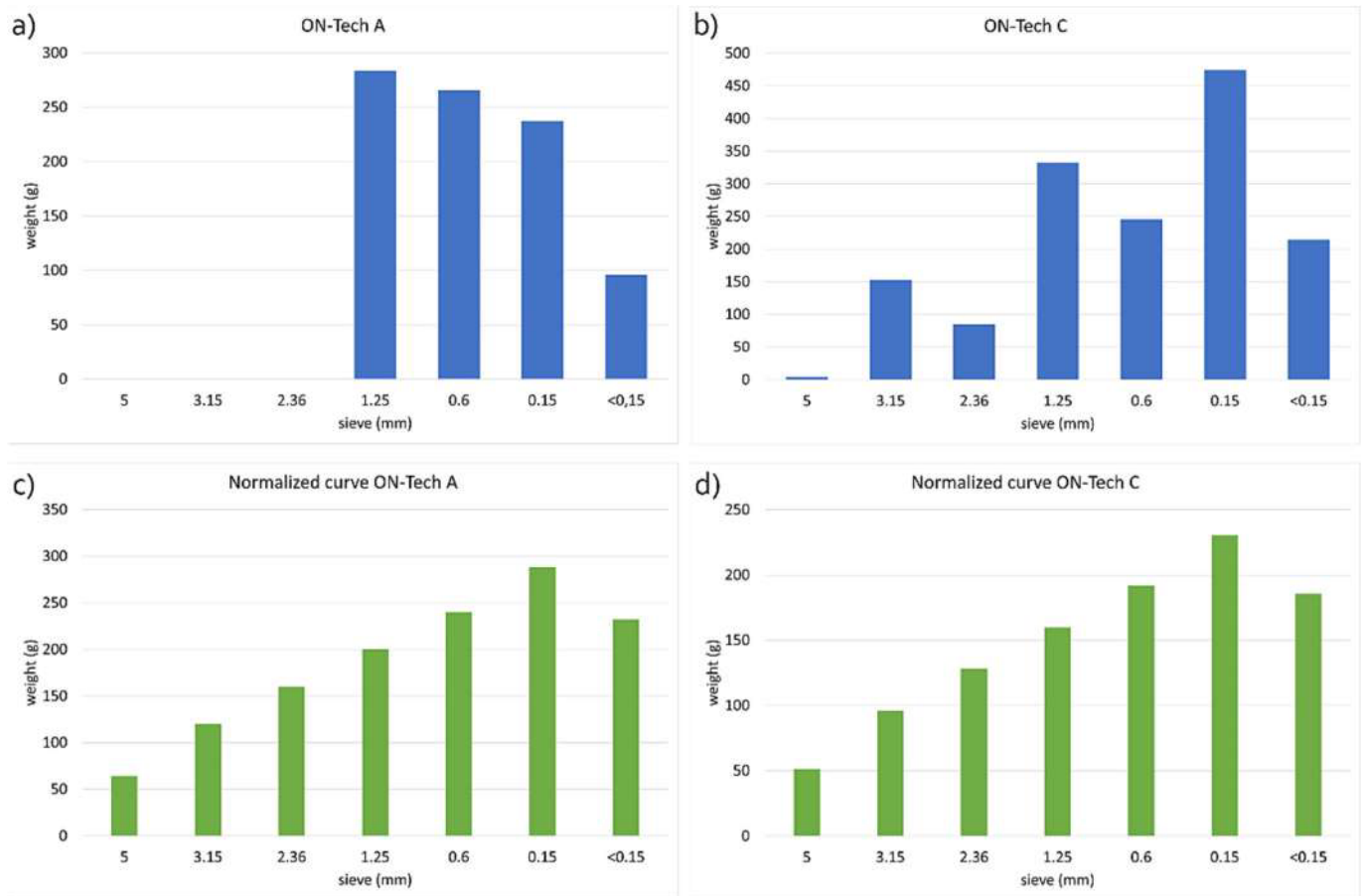Mortar specimens were produced by mixing the selected pozzolanic

Fig. 2. Grain size distribution of pozzolan materials (a and b) used in mortar specimens (c and d).

materials with two different natural hydraulic lime (NHL B and NHL D) (Table 2), following ASTM C305/UNI EN 196–1:2016 [37,38] (see Supplementary Materials SUP1).

According to the specific needs related to each methodology (see Section 2.3), specimens were produced as reported in Table SUP2.

2.3. Characterization of specimens

Mortar specimens were analysed using a multi-analytical approach, which included chemical, physical, biological, mineralogical and petrographic analyses.

OM, XRPD, SEM-EDS, and FTIR analyses were conducted for the mineralogical, petrographic and chemical characterization to investigate the phases formed during the setting reaction.

Specific surface area (BET method) and textural properties to assess micro- and mesoporosity in the mortar specimens were determined by the adsorption/desorption of N_2. The amount of absorbed water (H_2O wt %) and the kinetic of water desorption were determined by weighing mortars and Near-Infrared (NIR) Spectroscopy, respectively. Additionally, the distribution of pores accessible to water was non-invasively investigated using portable Nuclear Magnetic Resonance (NMR) Spectroscopy.

The NMR methods for investigating porous media rely on measuring the relaxation times and diffusion coefficients of water within the porous matrix [39–41]. Numerous experiments in the literature involving water-saturated rocks revealed that relaxation-time distributions often resemble pore-size distributions obtained through other methods like Mercury Intrusion Porosimetry (MIP). It is important to note that this similarity is not universal, given that NMR measures the size of pore bodies, while MIP measures the size of pore throats. Specifically, the transverse relaxation times T_2, of fluids confined in porous media are intricately linked to the structure's geometry. Water in small pores exhibits rapid relaxation, while water in large pores relaxes more slowly (i. e., the longer the T_2 value the greater the pore size).

Mechanical characterization of materials is an essential step in the process of determining the characteristics of functional materials. To achieve adequate knowledge of the mechanical characteristics of the prepared specimens, compression and flexural tests were performed with the purpose of measuring the breaking load under both compressive and bending stress, according to the UNI EN 12390-3:2009 and UNI EN 12390-5:2009, respectively.

Finally, experiments on exposure of microalgae cultures to the experimental specimens were performed to verify whether toxicological effects on these cells can be observed, e.g., due to pH variations or the presence of compounds released through leaching [29]. The analyses were carried out according to the OECD guidelines. The model systems suggested in Annex 2 of the OECD included green algae, diatoms and

Table 2
Mortar specimens.

Specimens	Binder	Aggregate	Binder/ aggregate ratio	Days of hardening	Days of setting
1	NHL B	Pozzolan A	3:1	3	25
2	NHL D	Pozzolan A	3:1	3	25
3	NHL B	Pozzolan C	3:1	3	25
4	NHL D	Pozzolan C	3:1	3	25

cyanobacteria, as suitable model systems to be used. Among these, the choice fell on *Raphidocelis subcapitata*, a microalga quite sensitive to toxic substances and with a ubiquitous distribution, so widely exploited in ecotoxicology. Microalgae cells are widely used for toxicity bioassays for their easily cultured and sensitivity to organic and inorganic pollutants [42], as well as for the short duration of monitoring. The relevance of these phytotoxicity tests has been recognized internationally and numerous test guidelines have been published [36,43,44] and incorporated in various regulatory procedures. In particular, the OECD recommended including a growth-inhibition experiment with microalgae in the base-set of ecotoxicological growth-inhibition tests. Currently, this analysis is legally demanded for all the substances produced or imported in Europe exceeding 10 t/year (Annexes VII-X [45]). For all these reasons and to provide a complete characterization of the new mortars, this type of analysis was included among the methodologies used.

2.4. Technical details of applied methods

Thin section OM was performed on pozzolan materials and mortar specimens using a Zeiss D-7082 Oberkochen polarized optical microscope in both parallel (PPL) and crossed polarized light (XPL). Micrographs at both PPL and XPL were performed using a Leica DM750 P microscope, with video camera Leica MC190 HD and LAS V4 4.12 software. Mortar specimens (SUP2) were described following the UNI 11176:2006 [46,47].

XRPD was performed on powder samples of pozzolan materials and mortar specimens (SUP2), gently pressed on a glass slide holder to minimize preferred orientation and analysed by a Bruker D8 Focus automated diffractometer with graphite-monochromatized Cu Kα radiation at 40 kV and 30 mA. Powder diffraction patterns were collected in step-scan mode from 3° to 60° 2θ, with a scan step-size of 0.02° in 2θ and 2 s of counting time. Data processing, including semi-quantitative analysis based on the "Reference Intensity Ratio Method", was performed using XPowderX© software. The identification of mineralogical phases was performed by the software using the ASCII PDF-2 commercial database published by the Joint Committee on Powder Diffraction Standards–International Centre for Diffraction Data (JCPDS–ICDD).

SEM-EDS analyses were performed on carbon-coated thin sections polished without cover glass of both pozzolan materials and mortar specimens (SUP2) using a FEI-Quanta 400 instrument, operating at 20 kV, equipped with X-ray energy-dispersive spectroscopy. Back Scattered Electron (BSE) images were collected along with EDS spectra of the aggregates and binder.

FTIR spectra were collected using a Nicolet iS50 FTIR Spectrometer. Samples of pozzolan and mortar specimens (SUP2) were gently scratched; the powder was deposited onto a diamond cell and analysed in Attenuated Total Reflection (ATR) mode. The spectra were collected in the range 4000–400 cm^{-1}, with a spectral resolution of 8 cm^{-1} and 40 scans were accumulated for each spectrum. The background was acquired on the air before each analysis, and a minimum of three analyses were performed for each specimen. Finally, the data processing was carried out using the OMNIC software©.

TG/DTA analysis were performed on natural hydraulic lime NHL B and NHL D and on mortar specimens (SUP2) in air using a heating rate of 10 °C/min and α-Al$_2$O$_3$ as a reference with a Netzsch Thermoanalyzer STA 409.

XRPD analysis on NHLs were performed by using a X'PERT diffractometer with CuKα radiation. Phase matching and pattern analysis were carried out using the X'Pert HighScore software from Panalytical.

Adsorption/desorption of N$_2$ at −196 °C was applied for each mortar specimen type (SUP2) using a Micromeritics 3Flex 3500 Analyzer (Norcross, GA, USA) after sample outgassing at 110 °C for 3.5 h via thermally controlled heating mantles, up to a residual pressure lower than 0.8 Pa. The pore distribution was determined by the BJH method [48] from the adsorption isotherm. The total pore volume was obtained

by the rule of Gurvitsch [49]. Supposing pores as cylindrical and considering the cylinder diameter as the pore size, the mortar pore size distribution curves show two maxima: one is referred as micropores, and the second one as mesopores. The uncertainty was ± 0.5 m^2·g^{-1} for the specific surface area values (BET method), ± 0.005 cm^3·g^{-1} for the total pore volume values, and ± 0.2 nm for the pore diameters.

The amount of absorbed water (H$_2$O wt%) was determined on mortar specimens (SUP2) as follows: samples were first dried under vacuum, at 90 °C, for 72 h (labelled as "dry") and then incubated, for 72 h, at 97 % relative humidity (in contact with vapours of a K$_2$SO$_4$ saturated solution at 25 °C, labelled as "97 % RH"). For each type of mortar, the following ratio was calculated on 3 different mortar portions:

$$(H_2O \text{ wt\%}) = [\text{weight (97\%RH)} - \text{weight (dry)}] \times 100/\text{weight (dry)}$$

NIR reflectance spectra were acquired over time, in reflectance mode, after incubation at 97 % RH, with a Varian Cary 5E spectrophotometer equipped with a LabSphere® Integrating Sphere System in the range 1850–2100 nm (1 nm step, 0.5 s averaging time, scan speed 120 nm/min) to measure water desorption kinetics for the different mortars. Once acquired as %R, the spectra were converted to log(1/R) using the SpectraGryph 1.2.16 software. Samples (SUP2) were exposed to air at 25 °C, to cover a time interval of approximately 20 h. The area of the NIR spectra, acquired at the various times, was normalized by the area of the NIR spectrum of the initial sample (97 % RH); such a normalization allowed the desorption kinetics comparison among the different mortar specimens. In order to explore further differences, NIR measurements were also performed for dry mortars and for other % RH values, obtained by exposition of mortar samples to vapours of saturated solutions of different salts, for 72 h, at 25 °C, namely: 33 % (saturated solution of MgCl$_2$•6H$_2$O), 51 % (saturated solution of Ca(NO$_3$)$_2$•6H$_2$O) and 79 % (saturated solution of NH$_4$Cl).

NMR analysis was carried out using a unilateral NMR instrument from Bruker Biospin interfaced with a single-sided sensor by RWTH Aachen University (Aachen, Germany) [50]. This sensor generates a magnetic field of 0.4 Tesla, with an extremely uniform gradient to resolve the near surface structure of arbitrary large samples. A Carr Purcell Meiboom Gill (CPMG) pulse sequence [51] was employed, with an echo-time (TE) of 57 μs, a time domain of 2048 echoes, and 1024 scans. The samples (SUP2) were measured using an RF coil operating at 13.62 MHz after undergoing saturation with water through full immersion for a duration of 72 h. To capture potentially variations in the microstructure of the mortar specimens, the measurements were taken at depths of 2.5 and 5 mm within the sample, respectively, with a sensitive volume resolution of 60 μm. This approach allows one to investigate how properties change with depth, providing insights into factors like hydration, curing, or the distribution of cementitious compounds. The distribution of T$_2$ was obtained by applying a UPEN algorithm [52] [VDT1] (Matlab) to the echo train recorded by the CPMG pulse sequence. Within the distribution, the peak maxima correspond to the most probable T$_2$ values in milliseconds, while the peak areas signify the populations of water protons for each component (all data were reported in Table SUP7, where the integrated peak area is subsequently reported as weight W (%) of each component, and the sum of weights was normalized to 100 %).

Compression tests were performed on each mortar specimen type (SUP2) through the use of a presser that meets the specifications of the EN 196–1 standard [37] both in terms of press speed and press geometry. The presser is equipped with a rigid frame and a spherical hinge used to make uniform the distribution of the load between the two flat and parallel plates of the presser and the specimen.

Finally, phytotoxicity tests toward *R. subcapitata* (61.81 SAG) cells were carried out, and any type of slowing down or blocking of important physiological phenomena naturally occurring within microalgae cells (such as cell division, electronic transfer within the photosynthetic process, and reduction of the production of photosynthetic metabolites)

was monitored for 9 days. In detail, the tests were performed with liquid cultures grown in Bold's Basal Medium for freshwater algae (which is widely used, easy to prepare, economical and able to facilitate the maintenance of axenic cultures) and in triplicate with 4 treatments and 1 control sample (in the presence of the 4 mortar specimens and without mortar, respectively). The cultures were placed at 25 ± 1 °C, exposed to 24-h light (80 μE/m^2/s) and with an agitation of 150 *rpm*. A dedicated shaking incubator (Sartorius Certomat BS-1) was used for the growth of microalgae with temperature and lighting conditions regulation. During the test period (i.e., 9 days), these conditions were kept stable. The solutions in experimental flasks were sampled every day for the analyses required during the time course respecting sterility conditions. The effects of mortar specimens on microalgae cells were evaluated by monitoring: i) growth curves (absorption at 750 nm and cell count); ii) growth rate; iii) photosynthetic pigment content (spectroscopic analysis of total chlorophylls); and iv) maximum quantum yield of PSII photochemistry (Fv/Fm). The cell growth was monitored using an automated cell counter analysis (TC-10 Biorad), while the culture density at 750 nm was determined. The total content of chlorophylls was defined by spectrophotometric analysis at 652 nm, following extraction with 80 % acetone, and the photosynthetic efficiency measured by fluorimeter [53]. The F_v/F_m parameter was calculated as $F_v/F_m = (F_m − F_0)/F_m$, where F_v is the variable fluorescence, F_0 is the initial fluorescence level registered at 50 μs after the onset of illumination, and F_m is the maximum fluorescence.

The growth rate (GR) was calculated as:

$$GR(d^{-1}) = [ln\,(final\ cell\ number)] − [ln\,(initial\ cell\ number)]/d$$

while the inhibition of microalgal cultures were quantified using the following equation:

$$\%I = (\mu_c − \mu_t)/\mu_c \times 100$$

where:

d number of days

%I percent inhibition in average specific growth rate μ;

μ_c mean value for μ in the control sample;

μ_t mean value for μ in treated sample.

3. Results

3.1. Raw materials

Optical microscopy analysis allowed to define pozzolan A as a pyroclastic material, highly vesiculated, with a brown-red matrix (Fig. 3, a). Among the phenocrysts, leucite is abundant (about 120 μm in size), with radial and concentric inclusions and diffuse fine clinopyroxene (rare macro-crystals up to 1 mm). Porosity is abundant, with irregular and elongated shapes up to 4 mm. Rounded porosity is also present with a smaller size (200 μm).

XRPD results of pozzolan A confirmed the microscopic analysis, highlighting the predominance of clinopyroxene and leucite (Table 3). The matrix is hipocrystalline, rich in micro-crystals of clinopyroxene as observed by SEM-EDS.

Based on OM, pozzolan B can be defined as a pyroclastic rock with a hipocrystalline matrix, in which visible crystals are mainly composed of K-feldspars (Fig. 3, b). The phenocrysts are mainly represented by altered pyroxene (~3 mm), feldspars (~2.5 mm), amphiboles (~500 μm) and opaques. The porosity is scarce and irregular with medium size around 0.7 mm. XRPD analyses confirmed the complex composition including predominant K-feldspar, diffuse plagioclase, and the presence of mica and analcime (Table 3).

The chemical composition of phenocrysts was deeply studied by the means of SEM-EDS. Feldspars are mainly composed of Si, Al, K, Na and Ca, which in some cases is substituted by Ba. Clinopyroxenes show a composition close to that of augite and amphiboles which are composed of Si, Mg, Al, K, Fe, Ti and Na (and in some cases also Ca) (Fig. 4, a). The matrix is mainly composed of K-feldspar, fractured analcime and iron oxides (Fig. 4, b). Some glazed areas of the matrix are composed of Al and Si, with variation at the rim of pores enriched in Fe, Mn, Ca, Ti, P and K.

OM allowed defining pozzolan C as a pyroclastic vesiculated material with brown matrix and phenocrysts of altered clinopyroxene (max 1.1 mm) and euhedral leucite without inclusions (~ 200 μm) (Fig. 3, c). The porosity is composed of abundant irregular pores with a medium size of 1 mm in which glazed rims are observed. XRPD results confirmed dominant leucite and clinopyroxene and the presence of K-feldspar and analcime (Table 3).

SEM-EDS analysis of pozzolan B showed zoned clinopyroxene with variations of Al and Fe contents, which are higher in the core, and the presence of Ti only in the inner part of the crystal. Iron oxides are also identified (Fig. 4, c) dispersed in the hipocrystalline matrix. The glazed areas at the rim of vesicles have a composition close to that of leucite enriched in Na, Mg, Ca and Fe.

The three pozzolan types show very similar FTIR spectra with a broad peak around 1000 cm^{-1} and one around 750 cm^{-1}, suggesting the predominance of silicates. Specifically, pozzolan A and C are characterized by the presence of leucite as the main component due to the intensity of the band at around 775 cm^{-1} and clinopyroxene (bands at about 900 and 680 cm^{-1}). The only difference between the two spectra concerns the peaks at around 3400 and 1635 cm^{-1}, referable to the vibrations of the absorbed water, present in the largest amount in pozzolan A, probably due to the large pores observed. As demonstrated by the previous analyses, pozzolan B has no leucite, the large peak at 993 cm^{-1} is related to the high content of K-feldspar (mainly microcline). FTIR spectrum also shows the presence of clay minerals in pozzolan B (characteristic peaks at 3698, 3621, 1118, and 910 cm^{-1}) (Table 3 and Fig. SUP3).

Pozzolans A and C are very similar to each other. In particular, pozzolan A has large porosity, and it is characterized by the presence of both concentric and radial leucite, whereas pozzolan C shows leucite without radial inclusions and small irregular porosity. These two pozzolan types resemble the aggregate materials identified inside ancient Roman mortars from the Trajan aqueduct [33]. Pozzolan B shows different characteristics from the material constituting the ancient mortars; for this reason, only pozzolans A and C were chosen as starting materials on which to proceed with the preparation of the mortar specimens.

Binder was analysed to provide additional information on the composition with respect to that declared in the technical data sheets. The DTA curve corresponding to NHL B (Fig. 5, a), reveals two endothermic peaks associated with the thermal decomposition of Ca(OH)$_2$ at around 510 °C and, very likely, to the thermal decomposition of CaCO$_3$ at about 820 °C, respectively. In addition, the corresponding TG curves indicate a weight loss of about 8.7 % and 9.8 % for the first and second peak, respectively. Considering the theoretical weight loss due to the decomposition of CaCO$_3$ and Ca(OH)$_2$, it is possible to estimate that CaCO$_3$ is around 22 % and Ca(OH)$_2$ is around 36 % of the total mass of the sample, respectively. The remaining mass of the sample is formed by a mixture of silicates, as revealed by XRPD (SUP4).

Conversely, the DTA curve corresponding to NHL D (Fig. 5, b) exhibits one single endothermic peak at a temperature of around 520 °C, attributable to the thermal decomposition of Ca(OH)$_2$. Such endothermic peak is coupled with a mass loss of about 13.7 %, corresponding to about 56 % of the total mass (based on the ratio between the registered weight loss, i.e. 13.7 %, and the theoretical weight loss of pure calcium hydroxide into calcium oxide, i.e. 24.3 %). Furthermore, there are two small additional endothermic peaks at about 750 °C and 840 °C, coupled with two small mass losses (accounting for a total mass loss of about 2.5 %), which could be attributed to the presence of calcite (as also confirmed by XRPD, SUP4) whose amount is in the order of about 5 %. The remaining 40 % is formed by a mixture of silicates, similarly to
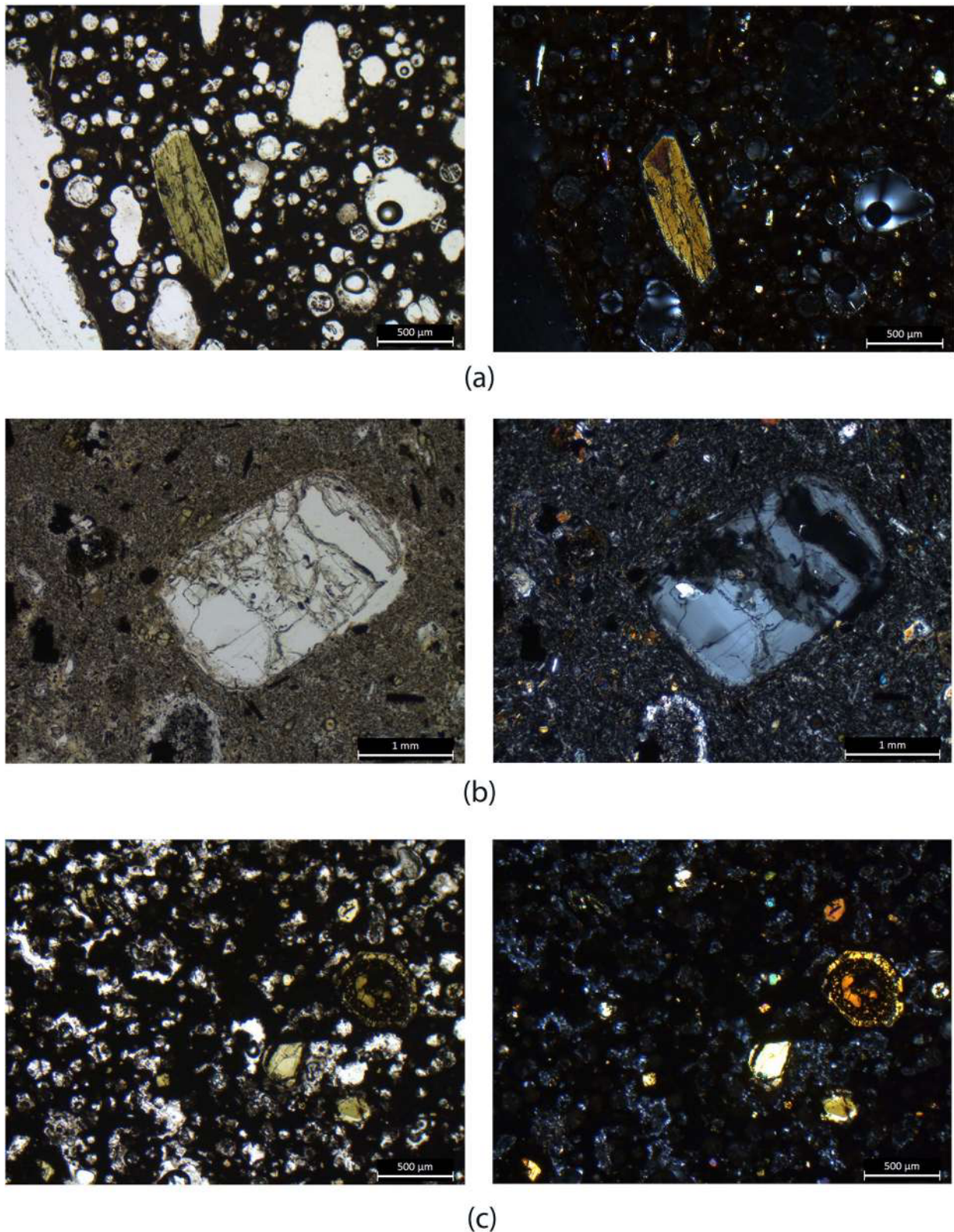
(a)

(b)

(c)

Fig. 3. Micrographs of the raw materials analysed at OM. Images (a) refers to pozzolan A (PPL on the left, XPL on the right): a phenocryst of clinopyroxene, with green core and yellow mantling rim at PPL, is visible, as well as crystals of leucite, with radial or concentric inclusions, in a brown-red matrix. Image (b) refers to pozzolan B (PPL on the left, XPL on the right): a phenocryst of feldspar, in an hipocrystalline matrix characterized by K-feldspars, clinopyroxenes and opaques. Images (c) refers to pozzolan C (PPL on the left, XPL on the right): on the right a phenocryst of clinopyroxene presents alteration, and other clinopyroxenes are present and green in colour at PPL; the matrix is dark brown, and pores have more irregular borders respect to pozzolan A. (For interpretation of the references to colour in this figure legend, the reader is referred to the web version of this article.)

Table 3
Results of XRPD and ATR-FTIR on pozzolan A, B and C (****very abundant 70–50 %, ***abundant 50–30 %, **present 30–15 %, *scarce 15–5 %, tr trace <5 %, − absent).

Pozzolan	Leucite	Clinopyroxene	K-feldspar	Plagioclase	Analcime	Mica	Clay minerals
A	****	***	−	−	−	−	−
B	−	tr	***	**	*	*	*
C	**	**	tr	−	tr	−	−

the other NHL. The relevant difference in terms of $Ca(OH)_2$ content could account for the different mechanical properties of the mortars specimens (as discussed below).

3.2. Characterization of mortar specimens

The analytical results confirmed the expected properties in chemical and mineralogical composition for the developed mortars given the raw materials and natural hydraulic lime, which were introduced in the mortar specimens.

Optical and electron microscopic analysis of all the specimens showed a calcitic lime binder. It shows a grayish brown colour, with neoformation hydraulic compounds, as they present the typical darker colour and irregular shape. Macro-porosity of all the specimens is abundant with spherical shape, ranging from 70 to 450 μm in specimen 1, from 115 to 450 μm in specimen 2, from 110 to 225 μm in specimen 3 and from 120 to 480 μm in specimen 4. The latter shows the maximum size of macro-pores close to those observed in ancient papal mortars from the *Aqua Traiana* aqueduct [33].

EDS analysis revealed a Si and Al enrichment at the interface between the aggregate and the binder (Fig. SUP5, a) as also observed in ancient papal mortars from the *Aqua Traiana* aqueduct [33], in all the four specimens, a bit more developed in mortar 4. In addition, only in the specimen 4, several white agglomerates consisting of micrometric regular crystals of calcium silico-aluminates are dispersed in the binder.

XRPD analysis and FTIR performed on the mortar specimens (Table 4 and Fig. 6) highlighted the high content of calcite, due to the binder fraction.

TG-DTA (SUP6) was performed to evaluate the hydraulic indices of the mortar specimens, calculated as the CO_2/H_2O ratio (weight loss of carbonates >600 °C respect to the weight loss of hydraulic water in the 200–600 °C range) [54,55]. The results in Table 5 highlight that specimen 4 has better hydraulic characteristics respect to the other mortar specimens here analysed [54,56,57] and values similar to papal mortars from the *Aqua Traiana* aqueduct (calculated as 2.55 in [34]).

Results of N_2 adsorption/desorption measurements, in terms of specific surface area, total pore volume, and maximum values in the pore size distribution, are reported in Table 6. All the mortar specimens are quite similar, but mortar 4 resulted slightly more porous, in terms of total pore volume, and with a higher specific surface area than the others, connecting to a higher water absorption (Table 6).

Water desorption kinetics by NIR reflectance spectroscopy are shown in Fig. 7 for all the mortar specimens. In the region 1850–2100 nm (Fig. 7) water has a broad absorption peak due to the -OH stretching and bending combination band, with a maximum centered at around 1940 nm (for pure liquid water). Mortar specimens 1, 2 and 3 behave similarly, reaching a water content comparable to that shown by the same specimens exposed to 79 % RH. Mortar specimen 4 shows a faster water desorption kinetic, reaching a water content well below 79 % RH (around 59 % RH).

Connecting to the absorbed water content, the distribution of pores accessible to the water was determined by NMR (Table SUP7). Across all mortar specimen types, a bimodal T_2 distribution is observed with two transverse relaxation times: a medium-short T_{2a} of approximately 1 ms with an average weight (W_a) component of 60 %, and a medium-long T_{2b} of 7 ms with an average weight (W_b) component of 40 %. In terms of pore size, the shorter T_{2a} value corresponds to water in the C-S-H

interlayer sheet spaces of the pores (nanometric scale), while the longer T_{2b} component is associated with water in the capillary pores of the structure (micrometric scale). Our results align well with data reported in literature [58] where the interlayer C-S-H pores ranging from 2 to 10 nm as well as capillary pores spanning from 50 to 600 nm. It is essential to note that the signal from water protons in crystalline water and OH-groups in C-S-H is not detectable by portable NMR due to their fast relaxation $T_2 < 0.05$ ms.

Regarding the variation in the distributions of T_2 as a function of depth inside the mortar specimens, similar distributions of T_2 were observed in mortar 1, 2 and 3. On the contrary, mortar 4 shows a shift of both T_2 values toward higher ones, indicating a larger interlayer sheet spaces of the pores at a depth of 2.5 mm. Furthermore, at a depth of 2.5 mm, the weight (W_a) of the interlayer sheet spaces shifted to 70 % of its value, while W_b decreased to 30 % (Fig. 8). This shift suggests a higher water content in the C-S-H interlayer compared to the water in the capillary pores. In simpler terms, this implies that within specimen 4 there are differences in the distribution of water between the C-S-H interlayer and the capillary pores, and there are variations in the arrangement of interlayer pore spaces when compared to the other specimens.

The results of both average compressive and flexural tests (Table 7) are consistent with the mechanical strengths of common cement-based mortars [59], also considering the designated strength classes of natural hydraulic lime used to prepare the various specimens (Table 2).

Based on data collected during phytotoxicity tests of new mortars on microalgae cells, no changes on treated cultures compared to the control were observed in the main physiological parameters during the entire time course (Table SUP8). In particular, identical growth rates (GR = 0.1 for all analysed samples) were calculated by analysing the number of cells/mL as a function of time and consequently the inhibition percentage (I%) was not significant. In conclusion, the materials of the new formulations did not release any toxic substance within the medium of treated cultures, and for this reason, they can be considered non-toxic materials on the model microorganism tested.

4. Discussion

The mineralogical and petrographic composition of the newly synthesized mortars has proved to be mainly affected by the nature of the aggregate, whereas the presence of reaction phases has been mainly connected to the nature of the binder.

All the specimens show a mineralogical and petrographic composition mainly determined by the added pozzolan types with a difference in the calcite content; the calcite content is partly due to the carbonation of calcium hydroxide and partly already present in the commercial NHL products. The binder is mineralogically and microstructurally similar to that observed in the ancient papal samples with reaction rims at the interface between the aggregate and the binder.

Specimens 1 and 3 (with NHL B as binder) are characterized by a slightly smaller macro-porosity (specimen 1: 70 to 450 μm; specimen 3: 110 to 225 μm), similar size of micro-pores (2.0 nm) and lower values of absorbed water (between 6.80 ± 0.03 and 6.71 ± 0.03), whereas specimens 2 and 4 (with NHL D as binder) show large macro-porosity (specimen 2: 115 to 450 μm; specimen 4: 120 to 480 μm), similar size of micro-pores (1.9 nm), higher water absorption values (between 8.23 ± 0.04 and 9.32 ± 0.02) as well as larger presence of reaction phases,
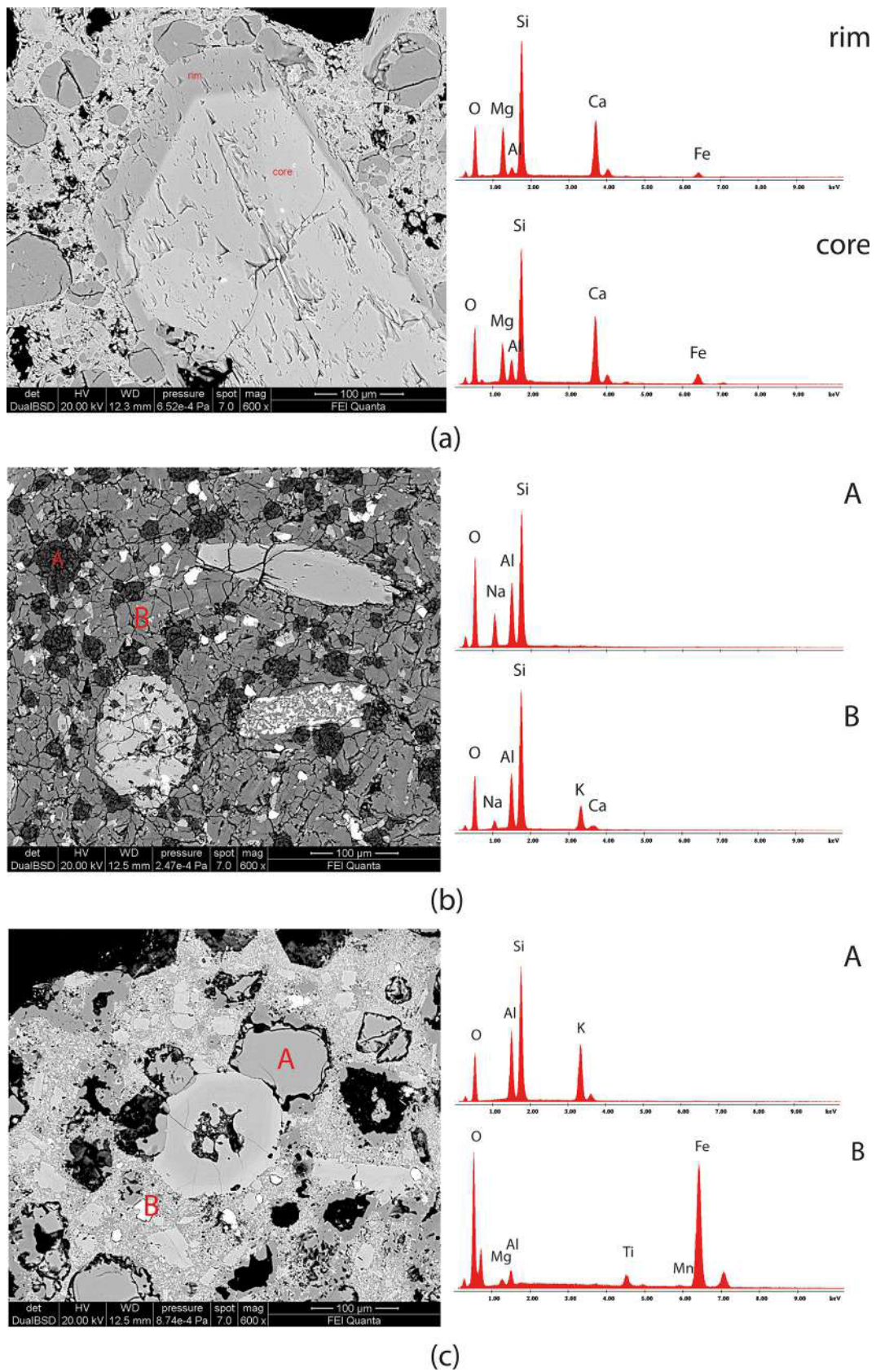
Fig. 4. SEM-BSE images and EDS spectra of the raw materials. (a) clinopyroxene (augite) shows chemical zoning that highlights an enrichment in Al and Fe in the core with respect to the rim in pozzolan A; (b) K-feldspar and fractured analcime in pozzolan B and (c) leucite and iron oxides dispersed in the hipocrystalline matrix in pozzolan C.
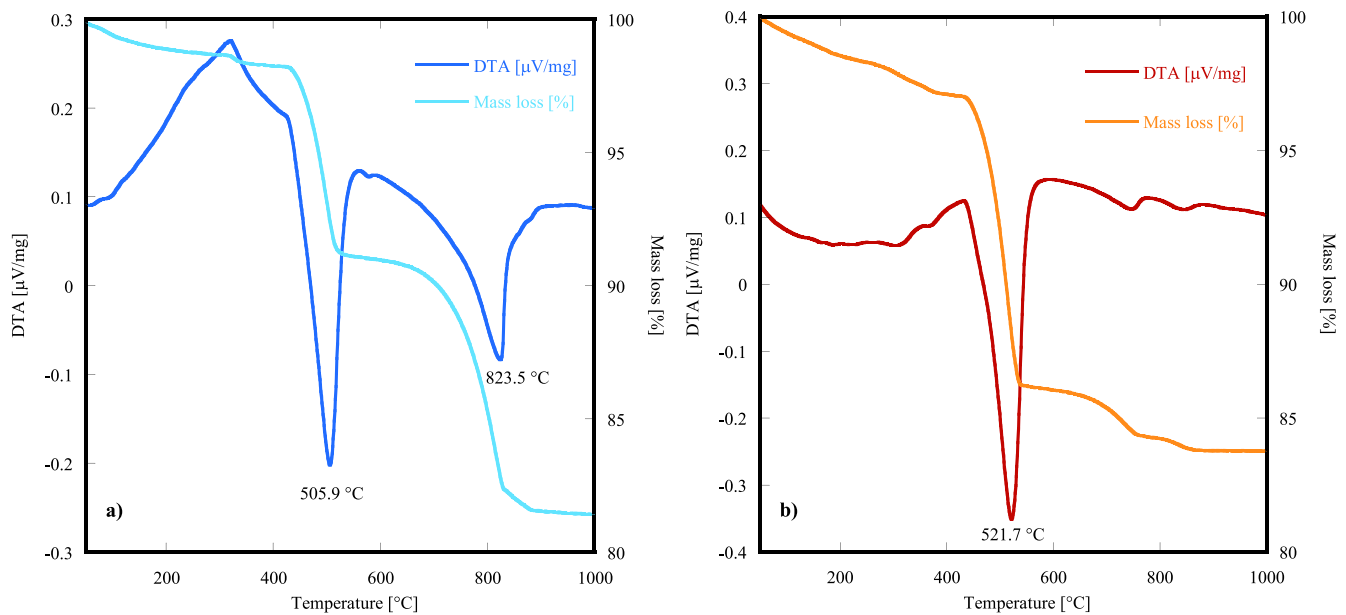
Fig. 5. DTA-TG curves of NHL-B (a) and NHL-D (b).

Table 4
XRPD results on the mortar specimens (****very abundant 70–50 %, ***abundant 50–30 %, **present 30–15 %, *scarce 15–5 %, tr trace <5 %, − absent).

New mortar	Calcite	Clinopyroxene	Leucite	Quartz
1	**	***	****	tr
2	*	***	***	−
3	**	**	****	−
4	**	****	**	−

and high hydraulicity behaviour.

Calcium silico-aluminates at the interface between the aggregate and binder have been identified much more present in specimens 2 and 4; additionally, in specimen 4 white agglomerates consisting of micrometric regular crystals are present. The large presence of reaction phases is attributed to the greater reactivity (compared to NHL B) of NHL D, which contains high amounts of portlandite, thus leading to a higher degree of alkali activation of the used pozzolan compared to all the other specimens. In addition, it is noteworthy that the formation of reaction phases is also connected to the presence of specific minerals as aggregate which can strongly influence the reactivity. Indeed, in specimen 4, the presence of analcimized leucite and glazed areas at the rim of pozzolan pores, due to the mixing of pozzolan C, can be considered an additional reason for this high reactivity.

The reactivity connected to the formation of newly formed phases is also confirmed by NMR analysis which shows, in mortar 4, a higher water proton density (W_a 70 %) in the interlayer C-S-H pores at the surface. Considering that the growth of these minerals creates a porous network inside the cement paste composed of C-S-H pores and capillary pores [60], our data confirm a potential more efficient reactivity in the formation of C-S-H compounds in specimen 4. The features of mortar 4 are also attested by N_2 adsorption/desorption measurements which pointed out textural properties that are typical for pozzolanic mortars, evidencing a slightly higher value of both specific surface area and total pore volume for the sample. Accordingly, mortar 4 is the one that has absorbed the highest amount of water and has showed the faster water desorption kinetic. Moreover, results of both average compressive and flexural tests indicate similar mechanical properties for each of the new proposed mortars, even though specimen 4 is the most performing one in terms of compressive strength, with a R_{cm} value almost 20 % higher than the average compressive strength of the other mortar specimens. This

behaviour can be associated with both the used NHL (in mortar 4, type D characterized by higher content of portlandite) and the peculiar pore structure as previously described.

The exploitation of the raw materials used in ancient times has driven to the formation of cement-free materials which are comparable with respect to the ancient ones from the mineralogical, petrographic and chemical point of view as well as to the hydraulic index value. The results can be a major boost in the direction of starting from the past to produce new future materials, as the new specimens show similar mechanical strength values of common cement-based mortars [59], further confirming the possible applicability of this material in the restoration field.

The enhanced macro and micro porosity, along with the increased specific surface area and total pore volume observed in specimen 4, can be attributed to the use of a more reactive pozzolan, due to the presence of analcimized leucite and glazed areas at the rim of pozzolan pores. This not only facilitates a more efficient formation of C-S-H compounds but also results in an improvement in compressive strength, making mortar 4 the most performing among the specimens examined in this study.

Being central the idea to produce green materials, ensuring safety to humans and environment, the evaluation of the phytotoxicity of the newly synthesized mortars allowed excluding their toxicity on *R. subcapitata* exposed to direct contact with them. Specifically, it was possible to exclude the leaching of chemicals or particles, into the culture medium by the new materials, capable of slowing down the growth speed of algae and in general negatively influencing their process of photosynthesis, cell division, and the production of chlorophylls. However, it is important to highlight that phytotoxicity on microalgae cells represents only part of the information required to define an eco-friendly product. Other information needs to be determined, such as physico-chemical features (e.g., leaching tests), as well as the ecotoxicological effects on various test organisms of different trophic levels.

New mortars have been produced based on the ancient materials which proved to have an extraordinary resistance to decay processes. It is noteworthy that the synthetic materials have been produced considering only a low number of variables (2 aggregates and 2 binders) and the use of commercial binders. The conscious choice to limit the number of variables was due to the need of finding a relationship between specific aggregate + binder with physical and mechanical features of the final product to better interpret the results. However, in the real mortars, the aggregate is a result of various volcanic materials, therefore it is
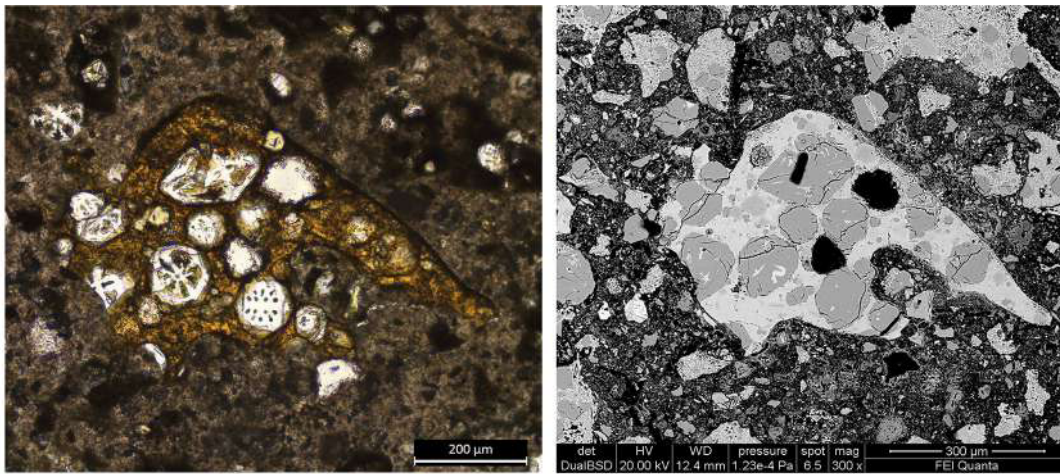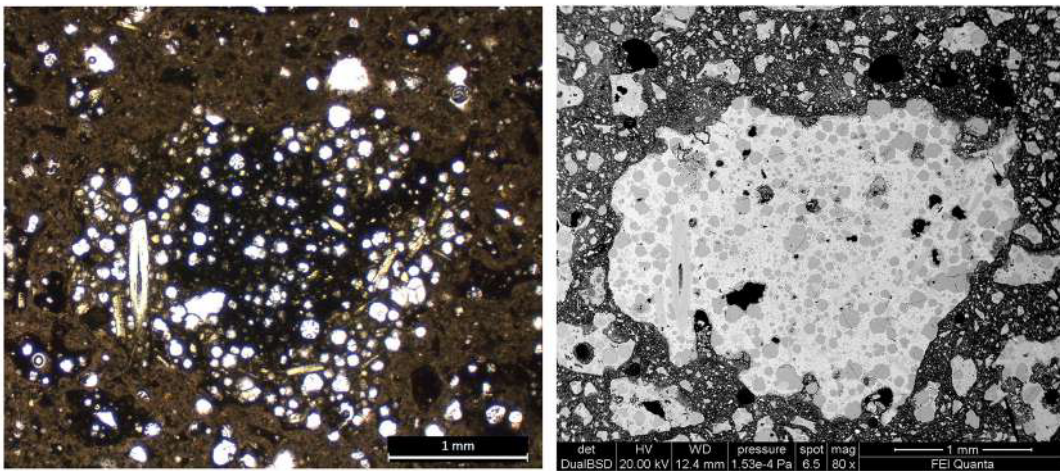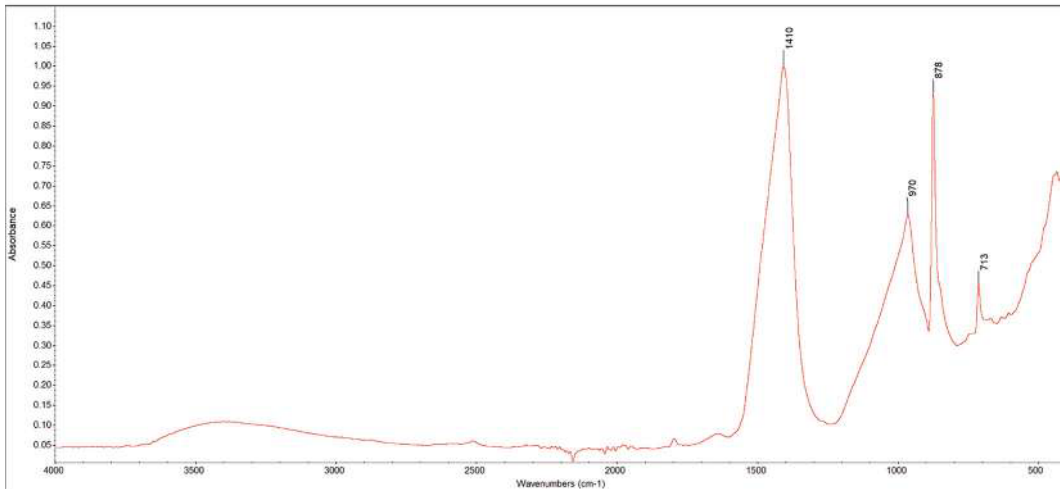
Fig. 6. OM microphotographs, SEM-BSE images and ATR spectrum of mortar specimens 1 (a) and 2 (b). (a) some aggregate fragments with glassy matrix and leucite crystals, in a binder with micritic texture, brown colour and small dark neoformation phases typical of natural hydraulic lime (PPL); (b) pozzolan consisting of leucite phenocrysts, rare clinopyroxene phenocrysts (one visible on the left) in a micritic binder, brown in colour (PPL); (c) presence of calcite (characteristic peaks at about 713, 878 and 1410 cm^{-1}) and leucite content highlighted by the intense peak at 970 cm^{-1}. (For interpretation of the references to colour in this figure legend, the reader is referred to the web version of this article.)

Table 5
Registered weight losses in the temperature intervals $T < 200$ °C (adsorbed water evolution), 200 °C $< T < 600$ °C (dehydration of hydrated silicoaluminates), $T > 600$ °C (C-S-H dehydration and calcium carbonate decomposition) and the CO_2/H_2O ratio.

Sample	Weight loss (wt%) in each temperature range (°C)			CO_2/H_2O ratio
	<200	200–600	>600	
1	2	2	8	4
2	2	2	7.5	3.75
3	2	2	9.5	4.75
4	3	3	7	2.3

Table 6
BET specific surface area (S.A.), total pore volume (V_{tot}), maximum values of pore diameter (D: the first value is referred to micropores, the second one to mesopores) and water absorption (wt%).

New mortar	S.A. ($m^2 \cdot g^{-1}$)	V_{tot} ($cm^3 \cdot g^{-1}$)	D (nm)	Absorbed water (H_2O wt%)
1	8.3	0.039	2.0; 18	6.80 ± 0.03
2	9.1	0.042	1.9; 18	8.23 ± 0.04
3	9.7	0.048	2.0; 20	6.71 ± 0.03
4	10.5	0. 052	1.9; 20	9.32 ± 0.02

important to highlight that the mortar specimens are not the real copy of ancient materials, but products obtained utilizing some of the same raw materials. The characterization of the mortar recipes proved that the produced mortar specimens, even if not copies, are similar to the ancient papal mortars, and consequently more compatible with old materials than cement-based products. In addition, they are safe for both the operators and the environment and exhibit resistance comparable to cement-based mortars.

The results of this study have highlighted the potential application of the mortar 4 in the restoration field as probably more compatible than cement-based materials, safe and resistant. However, application tests in various environments and monuments with different composition are needed to better evaluate the product. In addition, the specimens also need a comparison with respect to other restoration hydraulic mortars diffusely applied in the field.

The novelty of this work is therefore the methodology proposed here, starting from the study of the past to find new solution for the future, a perspective that, even with some limits, can represent a boost in the development of new, environmentally friendly products based on a sustainable approach.

5. Conclusions

The understanding of the raw materials used in the ancient Roman mortar production, the technological ancient knowledge and the chemical properties can disclose important information about the exceptional resistance and endurance of those materials, helping in the evaluation of new sustainable approaches applicable to modern mortars.

The methodology here proposed includes a first step of chemical and mineralogical characterization of ancient mortars on ancient monument showing exceptionally features in terms of durability and high technological level. The results are used to address the choice of the raw materials, meant as the nature of the binder, aggregate and the distribution grain size. The analytical results on chosen starting materials further indicate which types were similar to the old mortars. Starting from these data, new mortar recipes were produced and characterized in depth.

In this scenario, mortar 4 has resulted to be the most performing material in terms of the highest porosity, absorption of water, efficient reactivity in the formation of C-S-H compounds, hydraulic index and compressive strength. In addition, testing related to the phytotoxicity suggested the lack of toxic effects on microalgae cells, proving that new mortar recipes are safe for the environment. Finally, the similarity with respect to the ancient papal materials of the *Aqua Traiana* aqueduct and the mechanical strength values close to common cement-based mortars support the possible applicability of this material in the restoration field.
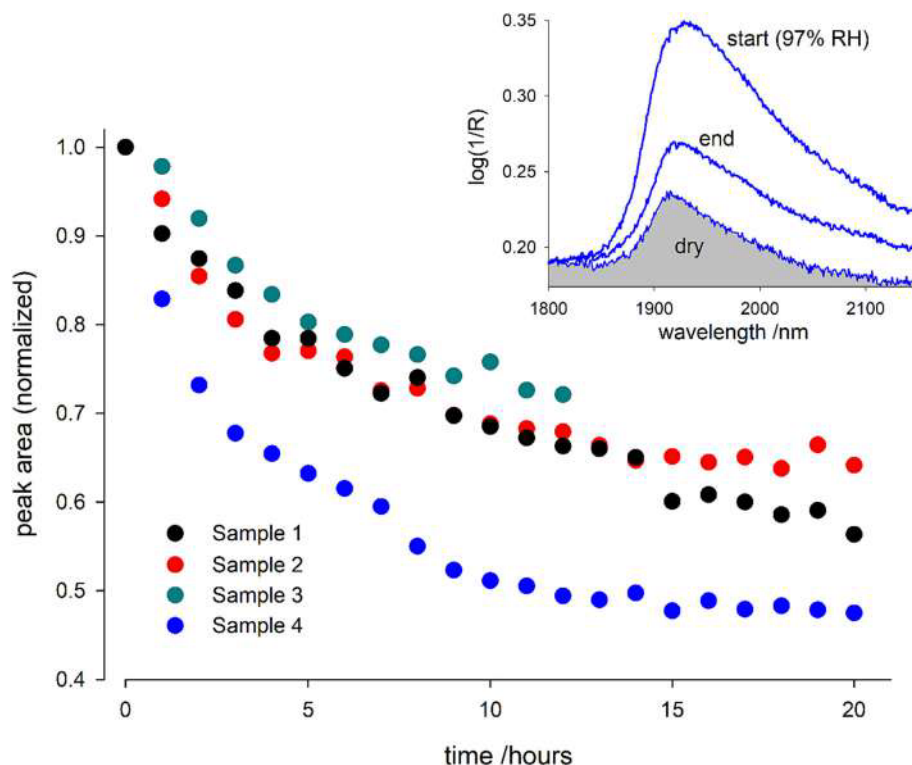

Fig. 7. Water desorption kinetics for the different mortars (see legend) as deduced by NIR reflectance spectroscopy. The inset shows relevant NIR spectra acquired for the mortar specimen 4 at the beginning and at the end of the kinetic experiments (the shaded NIR spectrum refers to the same sample when fully dried).
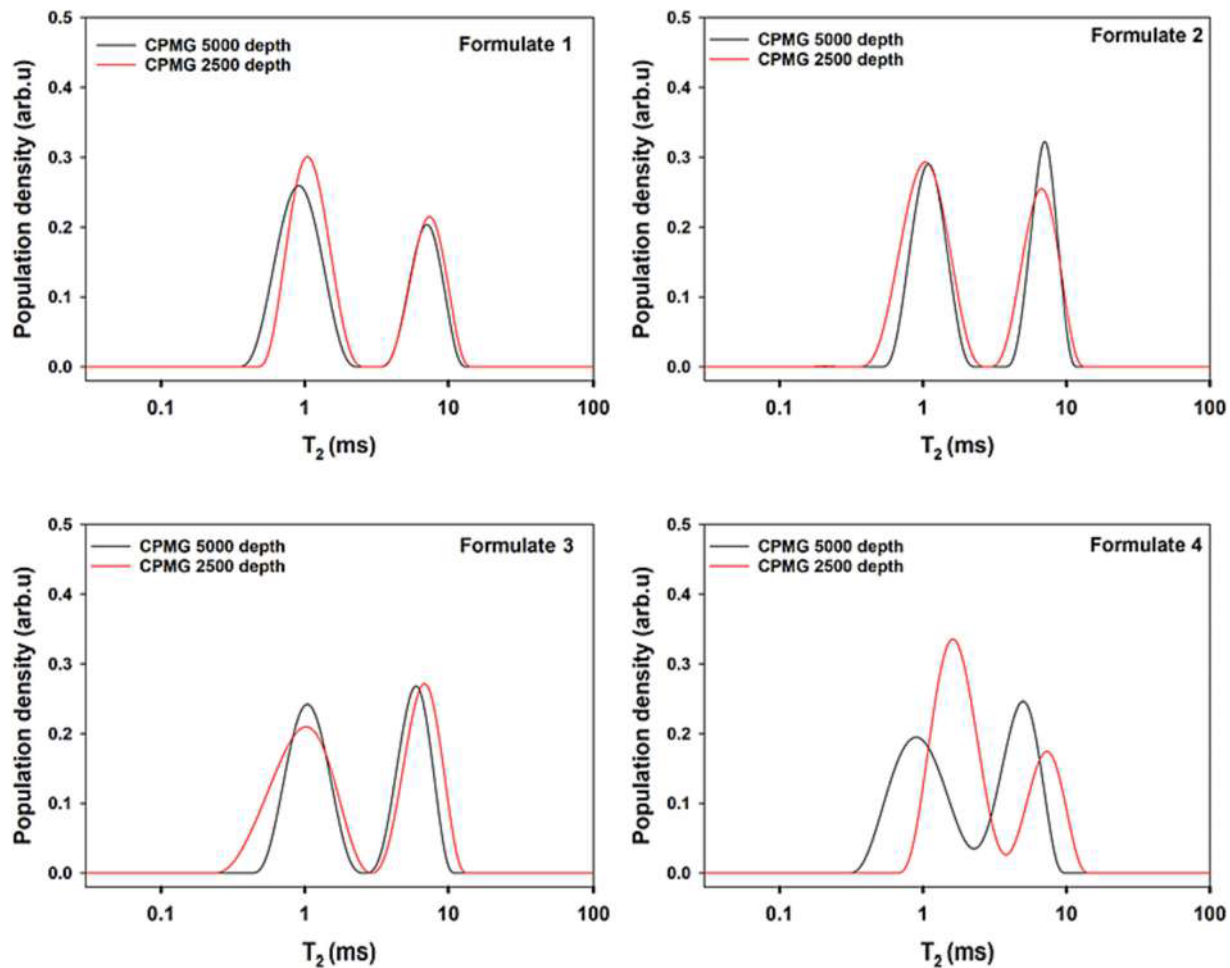
Fig. 8. Example of T_2 relaxation time distributions at a depth of 5 mm (black line) and 2.5 mm (red line) in the mortar specimens. (For interpretation of the references to colour in this figure legend, the reader is referred to the web version of this article.)

Table 7
Average compressive strength (R_{cm}) and flexural strength (R_{fm}) of the tested mortars.

New mortar	R_{cm} (MPa)	R_{fm} (MPa)
1	6.75	2.73
2	7.55	3.38
3	5.50	2.39
4	8.25	2.94

From this perspective, the new mortars can serve as appropriate materials for restoration applications in a sustainable preservation perspective of our past and our environment. To further assess their viability and commercialization, it is essential to conduct thorough evaluations and tests, taking into account the intended use in modern structures. This conservative approach ensures that these materials can be effectively adapted to meet the requirements of contemporary construction, retaining their valuable sustainability features.

CRediT authorship contribution statement

Laura Medeghini: Writing – original draft, Visualization, Supervision, Project administration, Methodology, Data curation, Conceptualization. **Laura Calzolari:** Writing – review & editing, Writing – original draft, Investigation. **Sara Capriotti:** Writing – original draft, Investigation. **Martina Bernabale:** Writing – original draft, Investigation. **Caterina De Vito:** Writing – review & editing. **Mauro Giustini:** Writing – review & editing, Visualization, Methodology, Funding acquisition. **Ida Pettiti:** Writing – review & editing, Writing – original draft, Visualization, Methodology, Investigation. **Gianfranco Dell'Agli:** Writing – review & editing, Writing – original draft, Visualization, Methodology, Funding acquisition, Formal analysis. **Luca Spiridigliozzi:** Writing – review & editing, Writing – original draft, Visualization, Investigation. **Amina Antonacci:** Writing – review & editing, Writing – original draft, Visualization, Methodology, Investigation, Funding acquisition, Formal analysis. **Giulia Gasperuzzo:** Writing – original draft, Investigation. **Viviana Scognamiglio:** Writing – review & editing. **Valeria Di Tullio:** Writing – review & editing, Writing – original draft, Visualization, Methodology, Investigation, Funding acquisition, Formal analysis. **Margherita Zappelli:** Writing – original draft, Investigation. **Lucia Conti:** Writing – review & editing. **Eleonora Gioventù:** Writing – review & editing. **Marina Marcelli:** Writing – review & editing. **Alfredo Bonaccini:** Visualization, Methodology, Investigation, Funding acquisition, Formal analysis. **Silvano Mignardi:** Writing – review & editing, Writing – original draft, Supervision, Project administration, Funding acquisition, Formal analysis, Conceptualization.

Declaration of competing interest

The authors declare that they have no known competing financial interests or personal relationships that could have appeared to influence the work reported in this paper.

Data availability

Data will be made available on request.

Appendix A. Supplementary data

Supplementary data to this article can be found online at https://doi.org/10.1016/j.cemconres.2024.107478.

References

[1] R.M. Andrew, Global CO_2 emissions from cement production, Earth Syst. Sci. Data. 10 (2018) 195–217, https://doi.org/10.5194/essd-10-195-2018.

[2] S.A. Miller, V.M. John, S.A. Pacca, A. Horvath, Carbon dioxide reduction potential in the global cement industry by 2050, Cem. Concr. Res. 114 (2018) 115–124, https://doi.org/10.1016/j.cemconres.2017.08.026.

[3] S.M. Borisov, C. Würth, U. Resch-Genger, I. Klimant, New life of ancient pigments: application in high-performance optical sensing materials, Anal. Chem. 85 (2013) 9371–9377, https://doi.org/10.1021/ac402275g.

[4] M.J. Melo, P. Nabais, M. Vieira, R. Araújo, V. Otero, J. Lopes, L. Martín, Between past and future: advanced studies of ancient colours to safeguard cultural heritage and new sustainable applications, Dyes Pigments 208 (2022) 110815, https://doi.org/10.1016/j.dyepig.2022.110815.

[5] P.A. Schroeder, G. Erickson, Kaolin: from ancient porcelains to nanocomposites, Elements 10 (2014) 177–182, https://doi.org/10.2113/gselements.10.3.177.

[6] M. Francis, L. King, V. Srinivasan, T. Purushothaman, Basalt fiber: an ancient material for innovative and modern application, Middle-East, J. Sci. Res. 22 (2014) 308–312, https://doi.org/10.5829/idosi.mejsr.2014.22.02.21872.

[7] J. Wadsworth, D.R. Lesuer, Ancient and modern laminated composites - from the great pyramid of Gizeh to Y2K, Mater. Charact. 45 (2000) 289–313, https://doi.org/10.1016/S1044-5803(00)00077-2.

[8] Z. Ye, P. Zhang, X. Lei, X. Wang, N. Zhao, H. Yang, Iron carbides and nitrides: ancient materials with novel prospects, Chem. Eur. J. 24 (2018) 8922–8940, https://doi.org/10.1002/chem.201706028.

[9] M.E. Rodriguez-Juarez, E. Perez-Diaz, G.I. Lopez-Dominguez, V.L. Picazo, D. Valencia-Cruz, B.M. Millan-Malo, M.E. Rodriguez-Garcia, Development and characterization of lime-based stucco for modern construction and restoration applications based on ancient stuccoes from the "El Cerrito" pyramid, Querétaro, Mexico, Case Stud. Constr. Mater. 16 (2022) e00875, https://doi.org/10.1016/j.cscm.2022.e00875.

[10] D. Medjelekh, A. Kenai, S. Claude, S. Ginestet, G. Escadeillas, Multi-technique characterization of ancient materials as part of an eco-renovation of historic centres, case of Cahors centre in France, Constr. Build. Mater. 250 (2020) 118894, https://doi.org/10.1016/j.conbuildmat.2020.118894.

[11] L.M. Seymour, D. Keenan-Jones, G.L. Zanzi, J.C. Weaver, A. Masic, Reactive ceramic aggregates in mortars from ancient water infrastructure serving Rome and Pompeii, Cell Reports Phys. Sci. 3 (2022) 101024, https://doi.org/10.1016/j.xcrp.2022.101024.

[12] L.M. Seymour, J. Maragh, P. Sabatini, M. Di Tommaso, J.C. Weaver, A. Masic, Hot mixing: mechanistic insights into the durability of ancient Roman concrete, Sci. Adv. 9 (2023) 1–13, https://doi.org/10.1126/sciadv.add1602.

[13] D.A. Silva, H.R. Wenk, P.J.M. Monteiro, Comparative Investigation of Mortars From Roman Colosseum and Cistern, Thermochim. Acta 438 (2005) 35–40, https://doi.org/10.1016/j.tca.2005.03.003.

[14] F. Marra, A. Danti, M. Gaeta, The volcanic aggregate of ancient Roman mortars from the Capitoline Hill: petrographic criteria for identification of Rome's "pozzolans" and historical implications, J. Volcanol. Geotherm. Res. 308 (2015) 113–126, https://doi.org/10.1016/j.jvolgeores.2015.10.007.

[15] E. Gotti, J.P. Oleson, C. Brandon, R. Cucitore, R.L. Hohlfelder, A comparison of the chemical and engineering characteristics of ancient Roman hydraulic concrete with a modern reproduction of vitruvian hydraulic concrete, Archaeometry 4 (2008) 576–590, https://doi.org/10.1111/j.1475-4754.2007.00371.x.

[16] M.D. Jackson, S.R. Chae, S.R. Mulcahy, C. Meral, R. Taylor, P. Li, A. Emwas, J. Moon, S. Yoon, G. Vola, H. Wenk, P.J.M. Monteiro, Unlocking the secrets of Al-tobermorite in Roman seawater concrete, Am. Mineral. 98 (2013) 1669–1687, https://doi.org/10.2138/am.2013.4484.

[17] M.D. Jackson, S.R. Mulcahy, H. Chen, Y. Li, Q. Li, P. Cappelletti, H.R. Wenk, Phillipsite and Al-tobermorite mineral cements produced through low-temperature water-rock reactions in Roman marine concrete, Am. Mineral. 102 (2017) 1435–1450, https://doi.org/10.2138/am-2017-5993CCBY.

[18] M.D. Jackson, J. Moon, E. Gotti, R. Taylor, S.R. Chae, M. Kunz, A. Emwas, C. Meral, P. Guttmann, P. Levitz, H. Wenk, P.J.M. Monteiro, Material and elastic properties of Al-tobermorite in ancient Roman seawater concrete, J. Am. Ceram. Soc. 2606 (2013) 2598–2606, https://doi.org/10.1111/jace.12407.

[19] A. Palomo, P. Monteiro, P. Martauz, V. Bilek, A. Fernandez-Jimenez, Hybrid binders: a journey from the past to a sustainable future (*opus caementicium futurum*), Cem. Concr. Res. 124 (2019) 105829, https://doi.org/10.1016/j.cemconres.2019.105829.

[20] M. Stefanoni, U. Angst, B. Elsener, Corrosion rate of carbon steel in carbonated concrete – a critical review, Cem. Concr. Res. 103 (2018) 35–48, https://doi.org/10.1016/j.cemconres.2017.10.007.

[21] U.M. Angst, Steel corrosion in concrete – Achilles' heel for sustainable concrete? Cem. Concr. Res. 172 (2023) 107239–107247, https://doi.org/10.1016/j.cemconres.2023.107239.

[22] A. Er, Ş. Kayış, Acute toxicity of pozzolanic cement on two crustacean species, water flea (*Daphnia magna*) and *Gammarus komareki*, Bull. Environ. Contam. Toxicol. 108 (2022) 309–314, https://doi.org/10.1007/s00128-021-03345-x.

[23] B. Rey-Alvarez, B. Sanchez-Montanes, A. García-Martínez, Building material toxicity and life cycle assessment: a systematic critical review, J. Clean. Prod. 341 (2022) 130838, https://doi.org/10.1016/j.jclepro.2022.130838.

[24] S. Accardo, S. Schiavo, L. Parrella, M. Rita, G. Lama, L. Verdolotti, S. Manzo, Do new cement-based mortars pose a significant threat to the aquatic environment? Chemosphere 332 (2023) 138818 https://doi.org/10.1016/j.chemosphere.2023.138818.

[25] N. Bandow, S. Gartiser, O. Ilvonen, U. Schoknecht, Evaluation of the impact of construction products on the environment by leaching of possibly hazardous substances, Environ. Sci. Eur. 30 (2018) 14, https://doi.org/10.1186/s12302-018-0144-2.

[26] H. Ali, E. Khan, I. Ilahi, Environmental chemistry and ecotoxicology of hazardous heavy metals: environmental persistence, toxicity, and bioaccumulation, J. Chem. 219 (2019) ID 6730305.

[27] S.R. Hillier, C.M. Sangha, B.A. Plunkett, P.J. Walden, Long-term leaching of toxic trace metals from Portland cement concrete, Cem. Concr. Res. 29 (1999) 515–521.

[28] W. Gwenzi, N.M. Mupatsi, Evaluation of heavy metal leaching from coal ash-versus conventional concrete monoliths and debris, Waste Manag. 49 (2016) 114–123, https://doi.org/10.1016/j.wasman.2015.12.029.

[29] K. Kobeticovà, R. Cerný, Ecotoxicology of building materials: a critical review of recent studies, J. Clean. Prod. 165 (2017) 500–508, https://doi.org/10.1016/j.jclepro.2017.07.161.

[30] A. Augustyniak, P. Sikora, J. Jablonska, K. Cendrowski, E. John, D. Stephan, E. Mijowska, The effects of calcium-silicate-hydrate (C–S–H) seeds on reference microorganisms, Appl. Nanosci. 10 (2020) 4855–4867, https://doi.org/10.1007/s13204-020-01347-5.

[31] I. Brás, P. Costeira, S. Ricardo, M.E. Silva, Recycling wastes in concrete production: performance and eco-toxicity assessment, Waste and Biomass Valor. 11 (2020) 1169–1180, https://doi.org/10.1007/s12649-018-0382-y.

[32] Comité européen de normalisation, CEN/TR 17105:2017, Construction Products – Assessment of Release of Hazardous Substances, 2017.

[33] M. Botticelli, L. Calzolari, C. De Vito, S. Mignardi, L. Medeghini, *Aqua Traiana*, a Roman infrastructure embedded in the present: the mineralogical perspective, Minerals 11 (2021), https://doi.org/10.3390/min11070703.

[34] L. Medeghini, L. Calzolari, M. Botticelli, M. Di Fazio, C. De Vito, I. Pettiti, F. Bardelli, S. Mignardi, The secret of ancient Roman hydraulic mortar: the lesson learnt from the past for future cements, Cem. Concr. Compos. (2024), https://doi.org/10.1016/j.cemconcomp.2024.105484, 105484 in press.

[35] M. Jackson, F. Marra, D. Deocampo, A. Vella, C. Kosso, R. Hay, Geological observations of excavated sand (*harenae fossiciae*) used as fine aggregate in Roman pozzolanic mortars, J. Rom. Archaeol. 20 (2007) 25–53, https://doi.org/10.1017/s1047759400005304.

[36] Organization for Economic Cooperation and Development, Test No. 201: Freshwater Alga and Cyanobacteria, Growth Inhibition Test, OECD Guidelines for the Testing of Chemicals, Section 2, 2011.

[37] Ente Italiano di Normazione e Comitato Europeo di Normazione, UNI EN 196-1: 2016 Methods of Testing Cement - Part 1: Determination of Strength, 2016.

[38] American Society for Testing and Materials, ASTM C305-20 Standard Practice for Mechanical Mixing of Hydraulic Cement Pastes and Mortars of Plastic Consistency, 2020.

[39] S. Chen, H.K. Liaw, A.T. Watson, Fluid saturation-dependent nuclear magnetic resonance spin-lattice relaxation in porous media and pore structure analysis, J. Appl. Phys. 74 (1993) 1473–1479.

[40] K.J. Dunn, D.J. Bergman, G.A. Latorraca, Nuclear Magnetic Resonance Petrophysical and Logging Applications, 1st ed, Pergamon, Elsevier Science, Oxford, 2002.

[41] A. Pop, I. Ardelean, Monitoring the size evolution of capillary pores in cement paste during the early hydration via diffusion in internal gradients, Cem. Concr. Res. 77 (2015) 76–81, https://doi.org/10.1016/j.cemconres.2015.07.004.

[42] T. Tato, R. Beiras, The use of the marine microalga *Tisochrysis lutea* (*T-iso*) in standard toxicity tests; comparative sensitivity with other test species, Front. Mar. Sci. 6 (2019) 488.

[43] A.S. for T. and Materials, ASTM E1218-04e1 Standard Guide for Conducting Static Toxicity Tests with Microalgae, (2004).

[44] ISO, ISO 10253:2006 Water Quality - Marine Algal Growth Inhibition Test With *Skeletonema costatum* and *Phaeodactylum tricornutum*. ISO. (2006).

[45] Registration Evaluation Authorisation and Restriction of Chemicals, Standard Information Requirements for Substances Manufactured or Imported in Quantities of 1000 Tonnes or More, 2006.

[46] Ente Italiano di Normazione, UNI 11176:2006 Beni culturali - Descrizione petrografica di una malta, 2006.

[47] E. Pecchioni, F. Fratini, E. Cantisani, Atlas of the Ancient Mortars in Thin Section under Optical Microscope, Nardini, 2017.

[48] P. Barrett, R. Skold, P. Barrett, Comparison between Nitrogen Isotherm and Mercury Porosimeter Methods 3, 1951, pp. 3155–3158.

[49] L. Gurvitsch, Physicochemical attractive force, J. Phys. Chem. Soc. Russ. 47 (1915) 805–827.

[50] J. Perlo, F. Casanova, B. Blümich, Profiles with microscopic resolution by single-sided NMR, J. Magn. Reson. 64–70 (2005).

[51] T.C. Farrar, E.D. Becker, Pulse and Fourier Transform NMR, Academic Press, New York, 1971.

[52] V. Bortolotti, R.J.S. Brown, P. Fantazzini, G. Landi, F. Zama, Uniform penalty inversion of two-dimensional NMR relaxation data, Inverse Probl. 33 (2017) 1–19, https://doi.org/10.1088/1361-6420/33/1/015003.

[53] A. Antonacci, M.D. Lambreva, A. Margonelli, A.P. Sobolev, S. Pastorelli, I. Bertalan, U. Johanningmeier, V. Sobolev, I. Samish, M. Edelman, V. Havurinne,

E. Tyystjärvi, M.T. Giardi, A.K. Mattoo, G. Rea, Photosystem-II D1 protein mutants of *Chlamydomonas reinhardtii* in relation to metabolic rewiring and remodelling of H-bond network at Q_B site, Sci. Rep. 8 (2018) 1–14, https://doi.org/10.1038/s41598-018-33146-y.

[54] A. Bakolas, G. Biscontin, A. Moropoulou, E. Zendri, Characterization of structural Byzantine mortars by thermogravimetric analysis, Thermochim. Acta 321 (1998) 151–160, https://doi.org/10.1016/s0040-6031(98)00454-7.

[55] G. Biscontin, M. Pellizon Birelli, E. Zendri, Characterization of binders employed in the manufacture of Venetian historical mortars, J. Cult. Herit. 3 (2002) 31–37, https://doi.org/10.1016/S1296-2074(02)01156-1.

[56] A. Moropoulou, A. Bakolas, K. Bisbikou, Characterization of ancient, byzantine and later historic mortars by thermal and X-ray diffraction techniques, Thermochim. Acta 269–270 (1995) 779–795, https://doi.org/10.1016/0040-6031(95)02571-5.

[57] P. Maravelaki-Kalaitzaki, A. Bakolas, A. Moropoulou, Physico-chemical study of Cretan ancient mortars, Cem. Concr. Res. 33 (2003) 651–661, https://doi.org/10.1016/S0008-8846(02)01030-X.

[58] R.M. Kowalczyk, A.M. Gajewicz, P.J. Mcdonald, The mechanism of water – isopropanol exchange in cement pastes evidenced by NMR relaxometry, RSC Adv. (2014) 20709–20715, https://doi.org/10.1039/c4ra00889h.

[59] M.M.T. Lakshani, T.K.G.A. Jayathilaka, J.A. Thamboo, Experimental investigation of the unconfined compressive strength characteristics of masonry mortars, J. Build. Eng. 32 (2020) 101558, https://doi.org/10.1016/j.jobe.2020.101558.

[60] A. Bede, A. Scurtu, I. Ardelean, NMR relaxation of molecules confined inside the cement paste pores under partially saturated conditions, Cem. Concr. Res. 89 (2016) 56–62, https://doi.org/10.1016/j.cemconres.2016.07.012.